

Pure Spin Current Injection in Hydrogenated Graphene Structures

Reinaldo Zapata-Peña,¹ Bernardo S. Mendoza,¹ and Anatoli I. Shkrebtii²

¹*Centro de Investigaciones en Óptica, León, Guanajuato 37150, México*

²*University of Ontario, Institute of Technology, Oshawa, ON, L1H 7L7, Canada*

(Dated: August 1, 2017)

Abstract

We present a theoretical study of spin-velocity injection of a pure spin current induced by a linearly polarized beam of light that impinges normally on the surface of two 50% hydrogenated noncentrosymmetric 2D graphene structures, labeled Up and Alt. The hydrogenation opens an energy gap in both structures. We analyze two possibilities: one in which by fixing the spin along a chosen direction, the resulting spin-velocity is calculated, and another where we choose the spin-velocity direction on the surface plane, and calculate its speed and spin orientation. We do so by changing the energy $\hbar\omega$ and polarization angle α of the incoming beam. The results are calculated within a full electronic band structure scheme within the DFT in the LDA approximation. The maxima of the spin-velocity speed are obtained when $\hbar\omega = 0.084$ eV and $\alpha = 35^\circ$ for Up, and $\hbar\omega = 0.720$ eV and $\alpha = 150^\circ$ for Alt. We find a speed of 668 Km/s and 645 Km/s for Up and Alt, respectively, when the spin points perpendicularly to the surface. Also, the response is maximized by fixing the spin-velocity direction along a high symmetry Cartesian axis, obtaining a speed of 688 Km/s with the spin pointing at 13° from the surface normal, for Up, and 906 Km/s and the spin pointing at 60° from the surface normal, for Alt. These speed values are larger than those of bulk semiconductors, like CdSe and GaAs, thus making the hydrogenated graphene structures excellent candidates for spintronics applications.

PACS numbers:

I. INTRODUCTION

Spintronics is an emerging research field of electronics in which the manipulation and transport of spin of electrons in a solid state media plays the determining role, adding a new degree of freedom to conventional charge manipulation.^{1,2} At present, there is an increasing interest in attaining the same level of control over the transport of spin at micro or nano scales, as it has been done for the flow of charge in typical electronic devices.³ Some semiconductor spintronics devices have been proposed^{4–7}, and some of them require spin polarized electrical current⁸ or pure spin current (PSC). One of the difficulties to achieve the development of spin current and PSC semiconductor devices is the fact that the spin relaxation time in a semiconducting media is short, disabling the spin transport, and then resulting in a non-observable spin current.⁹ In PSCs, there is no net motion of charge; spin-up electrons move in a given direction, while spin-down electrons travel in the opposite one. This effect can result from one photon absorption of linearly polarized light by a semiconductor, with filled valence bands and empty conduction bands, illuminated by light with photon energy larger than the energy gap. This phenomenon can result from spin injection,¹⁰ Hall Effects,¹¹ interference of two optical beams,^{12,13} or one photon absorption of linearly polarized light¹⁴ and has been observed in gallium arsenide (GaAs),^{15,16} aluminum-gallium arsenide (AlGaAs),¹⁶ and Co₂FeSi.¹⁷

Graphene, an allotrope of carbon with hexagonal 2D lattice structure, presents properties like fractional quantum Hall effect at room temperature, excellent thermal transport properties, excellent conductivity¹⁸ and strength^{19–22}, being then a perfect platform to be used in two-dimension electronic systems; however, most electronic applications are disabled by the absence of a semiconducting gap. Recent studies demonstrate that the band gap of graphene can be opened by applying an electric field,²³ reducing the surface area,²⁴ or applying uniaxial strain.²⁵ Another possibility to open the gap is by doping; this has been successfully achieved using nitrogen,²⁶ boron-nitrogen,²⁷ silicon,²⁸ noble-metals,²⁹ and hydrogen.^{30–32} Depending on the percentage of hydrogenation and spatial configurations of hydrogen-carbon bonds, hydrogenated graphene can result in different spatial configurations. In this paper, we present two 50% hydrogenated graphene noncentrosymmetric structures, both presenting a discernible band gap: the Up structure, shown in Fig. 1, has hydrogen atoms bonded to the carbon layer only on the upper side of the structure, while the Alt structure, shown in Fig. 2, has hydrogen alternating on the upper and bottom sides of the carbon slab.³³

Using those structures, we address a theoretical study of the spin velocity injection (SVI) by

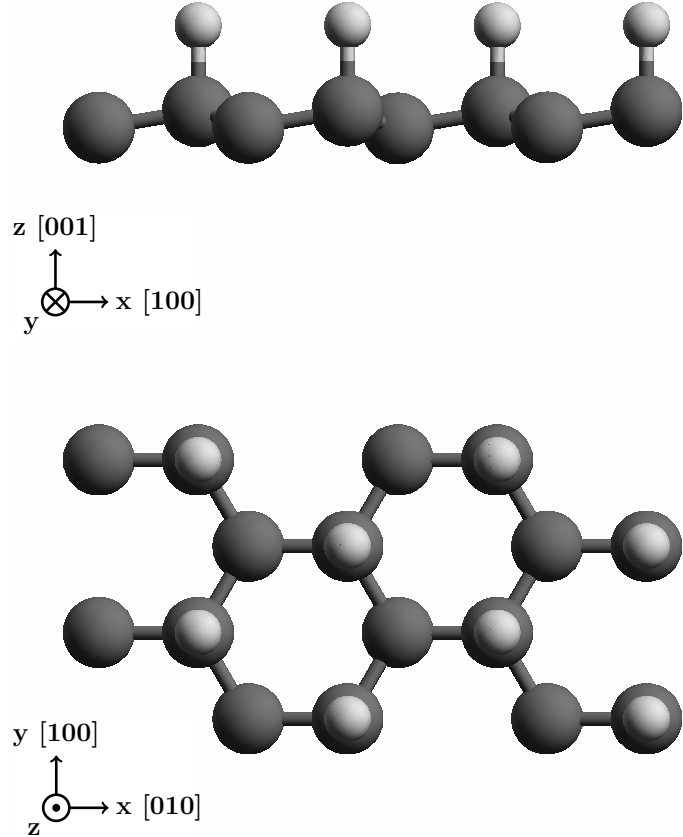


FIG. 1: Side (top panel) and top (bottom panel) views of the Up structure along with the Cartesian xyz directions. The dark (light) spheres are the C (H) atoms.

one-photon absorption of linearly polarized light. Since we have 2D structures, we do the analysis for two cases. The first is by fixing the spin of the electrons along the z Cartesian direction, with the velocity directed onto the surface of the structure on the xy plane. The second is by fixing the spin velocity in the x or y direction and the spin directed to xyz . The SVI is an optical effect that quantifies the velocity at which a PSC moves along the Cartesian direction, a , with the spin of electron polarized along the Cartesian direction b . One photon absorption of linearly polarized light can promote an even distribution of electrons in \mathbf{k} space, regardless of the symmetry of the material, resulting in a null electrical current.¹⁴ Then, the electrons excited to the conduction bands at opposite \mathbf{k} points will result in opposite spin polarizations producing no net spin injection.¹⁴ If the crystalline structure of the material is noncentrosymmetric, the spin polarization injected at a given \mathbf{k} point not necessarily vanishes,^{34,35} and then, since the velocities of

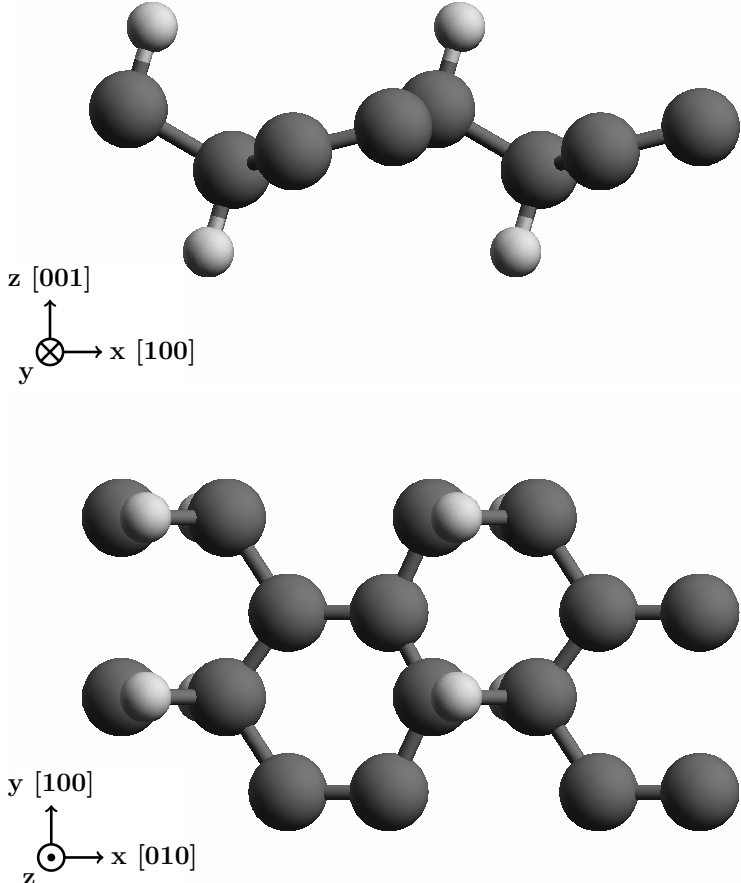


FIG. 2: Side (top panel) and top (bottom panel) views of the Alt structure along with the Cartesian xyz directions. The dark (light) spheres are the C (H) atoms.

electrons at opposite \mathbf{k} points are opposite, a PSC will be produced. Since the structures presented here are noncentrosymmetric, they are good candidates in which this effect can be induced.

This paper is organized as follows. In Section II we present the theory and formulas that describe PSC and SVI. In Section III we describe the details of calculations and the corresponding SVI spectra for the Up and Alt structures. Finally, we present our conclusions in Section IV.

II. THEORY

In this section, we report a summary of the theory involved in the calculation of the spin velocity injection (SVI) resulting from the pure spin current (PSC).

The operator that describes the electronic SVI is written as

$$\hat{K}^{ab} = \frac{1}{2} (\hat{v}^a \hat{S}^b + \hat{S}^b \hat{v}^a), \quad (1)$$

where $\hat{\mathbf{v}} = [\hat{\mathbf{r}}, \hat{H}_0]/i\hbar$ is the velocity operator, with $\hat{\mathbf{r}}$ being the position operator and \hat{H}_0 the unperturbed ground state Hamiltonian; the Roman superscripts indicate Cartesian coordinates. To obtain the expectation value of \hat{K}^{ab} , we use the length gauge for the perturbing Hamiltonian, written as

$$\hat{H}_p = -e\hat{\mathbf{r}} \cdot \mathbf{E}(t), \quad (2)$$

where the electric field of the applied laser is given by

$$\mathbf{E}(t) = \mathbf{E}(\omega)e^{-i\omega t} + \mathbf{E}^*(\omega)e^{i\omega t}. \quad (3)$$

In order to calculate the response of the system to $\mathbf{E}(t)$, one needs to take into account the excited coherent superposition of the spin-split conduction bands inherent to the noncentrosymmetric semiconductors considered in this work. To include the coherences, we follow Ref. 36 and use a multiple scale approach that solves the equation of motion for the single particle density matrix $\rho_{mn}(\mathbf{k}; t)$, leading to

$$\frac{\partial \rho_{cc'}(\mathbf{k})}{\partial t} = \frac{e^2 E^a(\omega) E^{b*}(\omega)}{i\hbar^2} \sum_v r_{cv}^a(\mathbf{k}) r_{vc'}^b(\mathbf{k}) \left(\frac{1}{\omega - \omega_{c'v}(\mathbf{k}) - i\epsilon} - \frac{1}{\omega - \omega_{cv}(\mathbf{k}) + i\epsilon} \right), \quad (4)$$

where we assumed that the conduction bands c and c' are quasidegenerate states, and we take $\epsilon \rightarrow 0$ at the end of the calculation. The spin-splitting of the valence (v) bands is very small, and is neglected throughout this work.³⁷ The matrix elements of any operator \mathcal{O} are given by $\mathcal{O}_{nm}(\mathbf{k}) = \langle n\mathbf{k} | \hat{\mathcal{O}} | m\mathbf{k} \rangle$, where $H_0|n\mathbf{k}\rangle = \hbar\omega_n(\mathbf{k})|n\mathbf{k}\rangle$ with $\hbar\omega_n(\mathbf{k})$ being the energy of the electronic band n at point \mathbf{k} in the irreducible Brillouin zone (IBZ), $|n\mathbf{k}\rangle$ is the Bloch state, and $\omega_{nm}(\mathbf{k}) = \omega_n(\mathbf{k}) - \omega_m(\mathbf{k})$. Using $\mathcal{O} = \text{Tr}(\hat{\rho}\hat{\mathcal{O}})$ for the expectation value of an observable \mathcal{O} , where Tr denotes the trace, we obtain

$$\mathcal{O} = \int \frac{d^3 k}{8\pi^3} \sum_{cc'} \rho_{cc'}(\mathbf{k}) \mathcal{O}_{c'c}(\mathbf{k}), \quad (5)$$

where we used the closure relationship $\sum_n |n\mathbf{k}\rangle \langle n\mathbf{k}| = 1$, where $n = v, c$, and the fact that $\rho_{vn}(\mathbf{k}) = \rho_{nv}(\mathbf{k}) = 0$ for $n = c, c'$. Therefore, using Eqs. (4) and (5), the rate of change of \mathcal{O} , $\dot{\mathcal{O}} = \text{Tr}(\dot{\hat{\rho}}\hat{\mathcal{O}})$, is given by

$$\dot{\mathcal{O}} = \frac{e^2}{i\hbar^2} \int \frac{d^3 k}{8\pi^3} \sum'_{cc'} \mathcal{O}_{c'c}(\mathbf{k}) r_{cv}^a(\mathbf{k}) r_{vc'}^b(\mathbf{k}) \left(\frac{1}{\omega - \omega_{c'v}(\mathbf{k}) - i\epsilon} - \frac{1}{\omega - \omega_{cv}(\mathbf{k}) + i\epsilon} \right) E^a(\omega) E^{b*}(\omega). \quad (6)$$

Replacing $\hat{O} \rightarrow \hat{K}^{ab}$, in the above expression, one can show that

$$\dot{K}^{ab}(\omega) = \mu^{abcd}(\omega) E^c(\omega) E^{d*}(\omega), \quad (7)$$

where repeated Cartesians are summed, and

$$\mu^{abcd}(\omega) = \frac{\pi e^2}{\hbar^2} \int \frac{d^3 k}{8\pi^3} \sum'_{vc,c'} \delta(\omega - \omega_{cv}(\mathbf{k}) \text{Re} \left[K_{cc'}^{ab}(\mathbf{k}) (r_{vc'}^c(\mathbf{k}) r_{cv}^d(\mathbf{k}) + (c \leftrightarrow d)) \right]) \quad (8)$$

is the pseudotensor that describes the rate of change of the PSC process in semiconductors. To derive what we presented above we used $K_{nm}^{ab}(-k) = K_{nm}^{ab*}(\mathbf{k})$ which follows from time-reversal invariance. The prime symbol ' in the sum means that c and c' are quasi degenerate states, and the sum only covers these states. Since $\mu^{abcd}(\omega)$ is real, we have that $\mu^{abcd}(\omega) = \mu^{abdc}(\omega)$. We remark that Eq. (8) is the same as Eq. (3) of Bhat et al.¹⁴, obtained by using the semiconductor optical Bloch equations. Using the closure relation,

$$K_{cc'}^{ab}(\mathbf{k}) = \frac{1}{2} \sum_{l=v,c} \left(v_{cl}^a(\mathbf{k}) S_{lc'}^b(\mathbf{k}) + S_{cl}^b(\mathbf{k}) v_{lc'}^a(\mathbf{k}) \right). \quad (9)$$

Now, we define the spin velocity injection (SVI) as

$$\mathcal{V}^{ab}(\omega) \equiv \frac{\dot{K}^{ab}(\omega)}{(\hbar/2)\dot{n}(\omega)}, \quad (10)$$

which gives the velocity, along direction a, at which the spin moves in a polarized state along direction b. The carrier injection rate $\dot{n}(\omega)$ is written as,³⁶

$$\dot{n}(\omega) = \xi^{ab}(\omega) E^c(\omega) E^{d*}(\omega) \quad (11)$$

where the tensor

$$\xi^{ab}(\omega) = \frac{2\pi e^2}{\hbar^2} \int \frac{d^3 k}{8\pi^3} \sum_{vc} r_{vc}^a(\mathbf{k}) r_{cv}^b(\mathbf{k}) \delta(\omega - \omega_{cv}(\mathbf{k})), \quad (12)$$

is related to the imaginary part of the linear optical response tensor by $\text{Im}[\epsilon^{ab}(\omega)] = 2\pi\epsilon_0\hbar\xi^{ab}(\omega)$.

The function $\mathcal{V}^{ab}(\omega)$ allows us to quantify two very important aspects of PSC. On one hand, we can fix the spin direction along b and calculate the resulting electron velocity. On the other hand, we can fix the velocity of the electron along b and study the resulting direction along which the spin is polarized. To this end, the added advantage of 2D structures, besides choosing them as noncentrosymmetric, is that we can use an incoming linearly polarized beam of light at normal incidence, and use the direction of the polarized electric field to control $\mathcal{V}^{ab}(\omega)$. Indeed, writing $\mathbf{E}(\omega) = E_0(\omega)(\cos\alpha \hat{\mathbf{x}} + \sin\alpha \hat{\mathbf{y}})$, where α is the polarization angle, we obtain from Eq. (10) that

$$\mathcal{V}^{ab}(\omega, \alpha) = \frac{2}{\hbar\xi(\omega)} \left(\mu^{abxx}(\omega) \cos^2 \alpha + \mu^{abyy}(\omega) \sin^2 \alpha + \mu^{abxy}(\omega) \sin 2\alpha \right), \quad (13)$$

for the structures chosen in this article, $\xi^{xx}(\omega) = \xi^{yy}(\omega) \equiv \xi(\omega)$, and $\xi^{xy}(\omega) = 0$. Now, we formalize our two options for $\mathcal{V}^{ab}(\omega)$.

A. Fixing spin

Analyzing the SVI, Eq. (13), we define the magnitude of the electron velocity on the plane of the structure, with the spin polarized along the b direction as

$$\mathcal{V}_{\sigma^b}(\omega, \alpha) \equiv \sqrt{[\mathcal{V}^{xb}(\omega, \alpha)]^2 + [\mathcal{V}^{yb}(\omega, \alpha)]^2}, \quad (14)$$

and define the angle at which the velocity is directed on the xy plane as

$$\gamma_{\sigma^b}(\omega, \alpha) = \tan^{-1} \left(\frac{\mathcal{V}^{yb}(\omega, \alpha)}{\mathcal{V}^{xb}(\omega, \alpha)} \right). \quad (15)$$

We also define two special angles

$$\gamma_{\sigma^b}^{\parallel}(\omega, \alpha) = \alpha, \quad (16)$$

and

$$\gamma_{\sigma^b}^{\perp}(\omega, \alpha) = \alpha \pm 90^\circ, \quad (17)$$

corresponding to the electron velocity being parallel or perpendicular to the incoming polarization, respectively. The subscript σ^b denotes the spin along b.

B. Fixing velocity.

Fixing the calculated velocity along $a = x$ or $a = y$, we define its corresponding magnitude as

$$\mathcal{V}_a(\omega, \alpha) \equiv \sqrt{[\mathcal{V}^{ax}(\omega, \alpha)]^2 + [\mathcal{V}^{ay}(\omega, \alpha)]^2 + [\mathcal{V}^{az}(\omega, \alpha)]^2}, \quad (18)$$

from where we see that the spin would be oriented in the xyz system's coordinates according to a polar angle

$$\theta_a(\omega, \alpha) = \cos^{-1} \left(\frac{\mathcal{V}^{az}(\omega, \alpha)}{\mathcal{V}_a(\omega, \alpha)} \right), \quad 0 \leq \theta \leq \pi, \quad (19)$$

and an azimuthal angle

$$\varphi_a(\omega, \alpha) = \tan^{-1} \left(\frac{\mathcal{V}^{av}(\omega, \alpha)}{\mathcal{V}^{ax}(\omega, \alpha)} \right), \quad 0 \leq \varphi \leq 2\pi. \quad (20)$$

Atom	Position (Å)		
	x	y	z
type			
H	-0.61516	-1.77416	0.73196
H	0.61518	0.35514	0.73175
C	-0.61516	-1.77264	-0.49138
C	-0.61516	-0.35600	-0.72316
C	0.61516	0.35763	-0.49087

TABLE I: Atomic positions in the unit cell of Up structure.

Atom	Position (Å)		
	x	y	z
type			
H	-0.61516	-1.42140	1.47237
C	-0.61516	-1.73300	0.39631
C	0.61516	1.73300	0.15807
C	0.61516	0.42201	-0.15814
C	-0.61516	-0.37396	-0.39632
H	-0.61516	-0.68566	-1.47237

TABLE II: Atomic positions in the unit cell of Alt structure.

III. RESULTS

We present the results of $\mathcal{V}_{\sigma^b}(\omega, \alpha)$ and $\mathcal{V}_a(\omega, \alpha)$ for the C₁₆H₈-up and C₁₆H₈-alt structures, being both noncentrosymmetric semi-infinite 2D carbon systems with 50% hydrogenation in different arrangements. We recall that the Up structure has hydrogen atoms only on the upper side of the carbon sheet, while the Alt structure has alternating hydrogen atoms on the upper and bottom sides. Also, we take the hexagonal carbon lattice to be on the xy plane for both structures, and the carbon-hydrogen bonds on the perpendicular xz plane, as depicted in Figs. 1 and 2. The coordinates for the Up and Alt unit cells of the structures are presented in Tables I and II.

We calculated the self-consistent ground state and the Kohn-Sham states using density functional theory in the local density approximation (DFT-LDA), with a planewave basis using the ABINIT code³⁸. We used Hartwigsen- Goedecker-Hutter (HGH) relativistic separable dual-space Gaussian pseudopotentials³⁹, including the spin-orbit interaction needed to calculate $\mu^{abcd}(\omega, \alpha)$ presented in Eq. (8). The convergence parameters for the calculations of our results corresponding

to the Up and Alt structures are cutoff energies of 40 Ha and 65 Ha, resulting in LDA energy band gaps of 0.084 eV and 0.718 eV, respectively. The energy eigenvalues and matrix elements for the Up and Alt structures were calculated using 12802 \mathbf{k} points and 14452 \mathbf{k} points in the IBZ to integrate $\mu^{abcd}(\omega)$ and $\xi^{ab}(\omega)$ using the linearized analytic tetrahedron method (LATM).³⁷ We neglect the anomalous velocity term $\hbar(\boldsymbol{\sigma} \times \nabla V)/4m^2c^2$, where V is the crystal potential, in $\hat{\mathbf{v}}$ of Eq. (1), as this term is known to give small contribution to PSC.¹⁴ Therefore, $[\hat{\mathbf{v}}, \hat{\mathbf{S}}] = 0$, and Eq. (1) reduces to $\hat{K}^{ab} = \hat{v}^a \hat{S}^b = \hat{S}^b \hat{v}^a$. Finally, the prime in the sum of Eq. (8) is restricted to quasidegenerated conduction bands c and c' that are closer than 30 meV, where this value is both a typical laser-pulse energy width and the room-temperature energy.³⁷

A. SVI: Spin velocity injection

In Fig. 3, we show $\mathcal{V}^{ab}(\omega, \alpha)$ vs. $\hbar\omega$ for the directions ab, and for the angle α that maximizes the signal, for the Up and Alt structures and for CdSe and GaAs, which are bulk systems shown for comparison. As expected from the delta function of Eq. (8), $\mathcal{V}^{ab}(\omega, \alpha)$ rises right at the corresponding energy gap of each system. For the 2D structures, the spectrum covers two narrow energy regions with large values of response, while for bulk systems, the spectra covers a rather wide energy range, but with a much smaller response. For the Up structure, ab = yz and $\alpha = 35^\circ$ maximize the response, which means that an incoming beam of light with its electric field polarized at 35° from the x direction will induce electrons to move along y (parallel to the surface), with their spin polarized along z (perpendicular to the surface), with the following speeds. Right at the energy onset, $\mathcal{V}^{yz}(\omega, \alpha) = 668$ Km/s, a speed that remains almost constant for 65 meV, and then goes to zero. A second region is found above 1.946 eV, where there are two extreme values of the speed, $\mathcal{V}^{yz}(\omega, \alpha) = 266.3$ Km/s at $\hbar\omega = 1.954$ eV, and $\mathcal{V}^{ab}(\omega, \alpha) = -241.4$ Km/s at $\hbar\omega = 1.958$ eV; a positive (negative) $\mathcal{V}^{ab}(\omega, \alpha)$ means that the electrons move parallel (antiparallel) to the electric field. Likewise, for the Alt structure, we find that also ab = yz and $\alpha = 150^\circ$ maximizes the response, where two extreme values of \mathcal{V}^{yz} are found, one at $\hbar\omega = 0.720$ eV of $\mathcal{V}^{yz} = -711.9$ Km/s, and the other at $\hbar\omega = 0.911$ eV of $\mathcal{V}^{yz} = -330.6$ Km/s.

For the bulk structures, we calculate $\mathcal{V}^{ab}(\omega)$ from Eq. (10) by simply using $\boldsymbol{\mu}_{\max}$. For CdSe, we find that for $\hbar\omega = 0.844$ eV, $\boldsymbol{\mu}_{\max} \rightarrow \mu^{zzzz}$, and $\mathcal{V}^{zz}(\omega) = -59.0$ Km/s, and for GaAs at $\hbar\omega = 2.324$ eV, $\boldsymbol{\mu}_{\max} \rightarrow \mu^{aaaa}$ and $\mathcal{V}^{aa}(\omega, \alpha) = -28.7$ Km/s, with $a = x, y, z$. For these bulk semiconductors, the x , y , and z axis are taken along the standard cubic unit cell directions, [100], [010], and [001], respectively. In Table III, we present the comparison of $\mathcal{V}^{ab}(\omega, \alpha)$ for the 2D

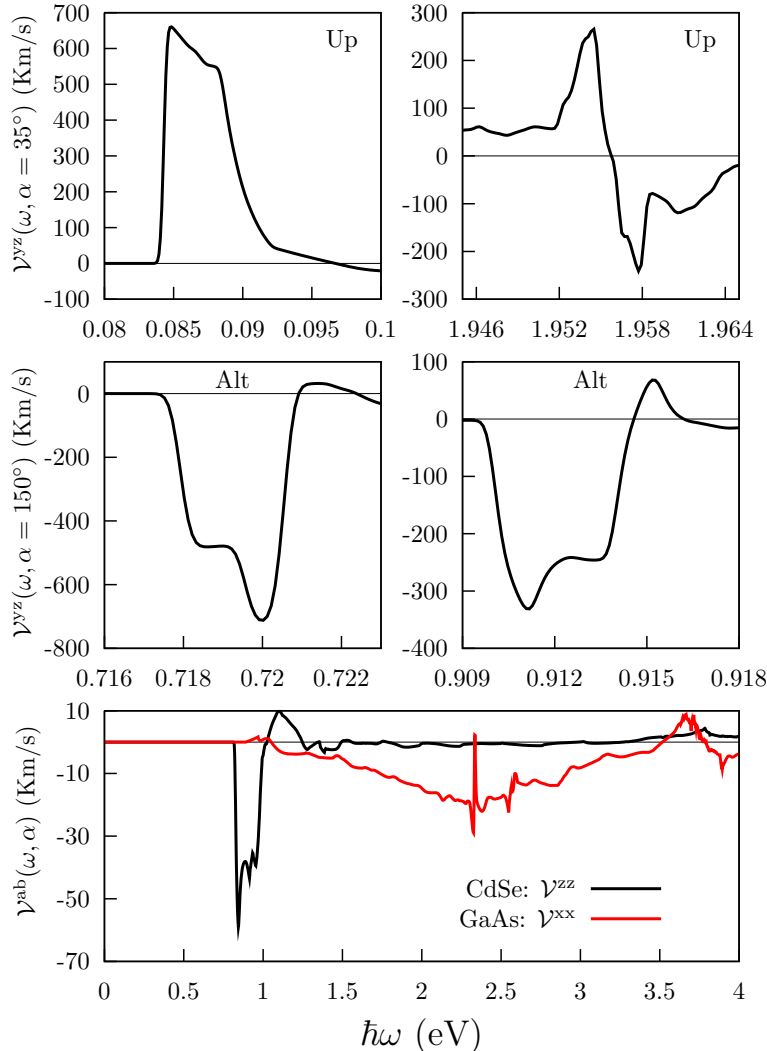


FIG. 3: $\mathcal{V}^{ab}(\omega, \alpha)$ vs. $\hbar\omega$, for the values of α that maximize the signal. The low energy regions for the Alt and Up structures start at the energy gap of each structure, while in the high energy regions, the values of $\mathcal{V}^{ab}(\omega, \alpha)$ are also very large. The bottom panel corresponds to CdSe and GaAs.

structures and bulk crystals. We remark that, as shown in the figure, the 2D structures have maxima in $\mathcal{V}^{ab}(\omega; \alpha)$ that are bigger than for the bulk crystals; in particular, the Alt structure gives a $\mathcal{V}^{ab}(\omega; \alpha) \sim 12$ times larger than that of CdSe and GaAs.

B. Fixing spin

In this subsection, we calculate $\mathcal{V}_{\sigma^z}(\omega, \alpha)$, Eq. (14), for the case where the spin is fixed along z , i.e. directed perpendicularly to the surface of the Up and Alt structures. Also, we calculate $\gamma_{\sigma^z}(\omega, \alpha)$, Eq. (15), which determines the direction along which the injected electrons move along

Structure	Kind of system	Pol. Ang.	Energy [eV]	$\mathcal{V}^{ab}(\omega, \alpha)$	
				ab	[Km/s]
Up	2D	35	0.084	yz	660.5
			1.954	yz	266.3
			1.958	yz	-241.4
Alt	2D	150	0.720	yz	-711.9
			0.911	yz	-330.6
CdSe	bulk	-	0.844	zz	-59.0
GaAs	bulk	-	2.324	xx	-28.7

TABLE III: Comparison of the reported maximum values of $\mathcal{V}^{ab}(\omega, \alpha)$ for the different structures and their corresponding polarization angle α and $\hbar\omega$ energy values.

the surface of each structure. We mention that we have also made the analysis for the cases when the spin is directed along x or y, finding similar qualitative results to those presented below.

1. Up structure

In the top panel of Fig. 4, we plot $\mathcal{V}_{\sigma^z}(\omega, \alpha)$ vs. $0.080 \text{ eV} \leq \hbar\omega \leq 0.096 \text{ eV}$ (similar energy range for the Up structure shown in the left panel of Fig. 3) and $0^\circ \leq \alpha \leq 180^\circ$. We see a broad peak that maximizes at $\alpha = 35^\circ$ and $\hbar\omega = 0.084 \text{ eV}$, with a value of $\mathcal{V}_{\sigma^z}(\omega, \alpha) = 739.7 \text{ Km/s}$, and that the variation of $\mathcal{V}_{\sigma^z}(\omega, \alpha)$ as a function of α , which comes from the interplay of the μ tensor components as multiplied by the trigonometric functions of Eq. (13), gives a sizable set of values between 739.7 Km/s and 165.4 Km/s, for $0.084 \text{ eV} \leq \hbar\omega \leq 0.090 \text{ eV}$. In the bottom panel, we show $\mathcal{V}_{\sigma^z}(\omega, \alpha)$ vs. α (left scale, black line), at $\hbar\omega = 0.084 \text{ eV}$, thus following the ridge shown in the 3D plot of the top panel. Also, we plot the corresponding velocity angle $\gamma_{\sigma^z}(\omega, \alpha)$ (right scale, red line), where it is very interesting to see that $\gamma_{\sigma^z}(\omega, \alpha)$ is centered at 64.55° with a rather small deviation of only $\pm 0.03^\circ$, for the whole range of α . This results means that for $\hbar\omega = 0.084 \text{ eV}$ and for all values of α , the electrons, with the chosen spin pointing along z , will move at an angle of $\gamma_{\sigma^z}(\omega, \alpha) \sim 64.5^\circ$ with respect to the x direction, with the range of high speeds $\mathcal{V}_{\sigma^z}(\omega, \alpha)$ shown in the figure. Also, from Eq. (16) we find that $\gamma_{\sigma^z}^{\parallel}(\omega, \alpha) = \alpha = 64.56^\circ$, with $\mathcal{V}_{\sigma^z}(\omega, \alpha) = 631.1 \text{ Km/s}$ (see green arrow), and that from Eq. (17), $\gamma_{\sigma^z}^{\perp}(\omega, \alpha) = \alpha - 90^\circ = 64.50^\circ$, gives $\alpha = 154.50^\circ$, with $\mathcal{V}_{\sigma^z}(\omega, \alpha) = 191.5 \text{ Km/s}$ (see blue arrow); thus, at $\hbar\omega = 0.084 \text{ eV}$, an incident field polarized at $\alpha \sim 65.5^\circ$ or $\sim 154.5^\circ$, injects electrons with their spin polarized along z , which move parallel or perpendicular to the incident electric field, with a speed of 631.14 Km/s or 191.5 Km/s, respectively.

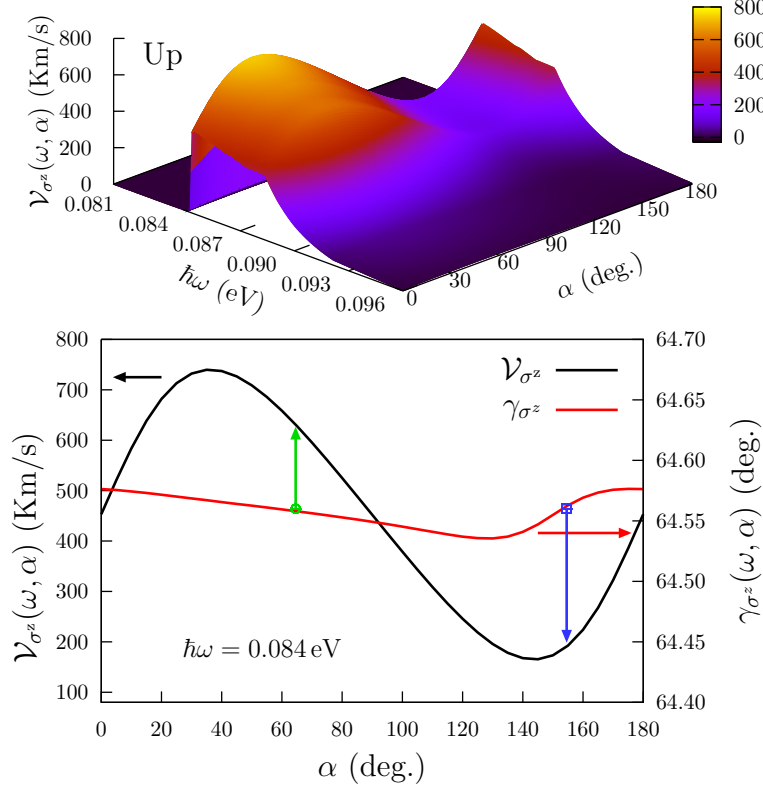


FIG. 4: For the Up structure, the top panel shows $\mathcal{V}_{\sigma^z}(\omega, \alpha)$ vs. $\hbar\omega$ and α , and the bottom panel shows $\gamma_{\sigma^z}(\omega, \alpha)$ (right scale, red line), and $\mathcal{V}_{\sigma^z}(\omega, \alpha)$ (left scale, black line), vs. α , for $\hbar\omega = 0.084$ eV, i.e. along the ridge shown in the 3D plot.

Now, we analyze the results for the second energy range of the Up structure shown in the top right panel of Fig. 3. In the top panel of Fig. 5, we plot $\mathcal{V}_{\sigma^z}(\omega, \alpha)$ vs. $1.950 \text{ eV} \leq \hbar\omega \leq 1.960 \text{ eV}$ and $0^\circ \leq \alpha \leq 180^\circ$. We see two broad peaks that maximize at $\alpha = 35^\circ$ and $\hbar\omega = 1.954$ eV, with a value of $\mathcal{V}_{\sigma^z}(\omega, \alpha) = 193.5$ Km/s, and at $\alpha = 35^\circ$ and $\hbar\omega = 1.957$ eV, with a value of $\mathcal{V}_{\sigma^z}(\omega, \alpha) = 170.6$ Km/s. We only analyze the highest maximum in the bottom panel, where we show $\mathcal{V}_{\sigma^z}(\omega, \alpha)$ vs. α (left scale, black line), at $\hbar\omega = 1.954$ eV, thus following the highest ridge shown in the 3D plot of the top panel. Also, we plot the corresponding velocity angle $\gamma_{\sigma^z}(\omega, \alpha)$ (right scale, red line), where in this case we see that the values of $\gamma_{\sigma^z}(\omega, \alpha)$ have more dispersion, as a function of α , than for the lower energy range shown in the bottom panel of Fig. 4. However, $\gamma_{\sigma^z}(\omega, \alpha) \sim 77.8^\circ$ is constant from $\alpha = 0^\circ$ and up to $\alpha \sim 85^\circ$. In this case, we find that $\gamma_{\sigma^z}^{\parallel}(\omega, \alpha) = \alpha = 78.0^\circ$, with $\mathcal{V}_{\sigma^z}(\omega, \alpha) = 115.0$ Km/s (see green arrow), and that from Eq. (17), $\gamma_{\sigma^z}^{\perp}(\omega, \alpha) = \alpha - 90^\circ = 167.8^\circ$, gives $\alpha = 77.8^\circ$, with $\mathcal{V}_{\sigma^z}(\omega, \alpha) = 65.6$ Km/s (see blue arrow). Thus, through the correct choice of $\hbar\omega$ and α we could inject electrons, in this case with their spin polarized along z , which move parallel or perpendicular to the incident electric field, with finite speeds.

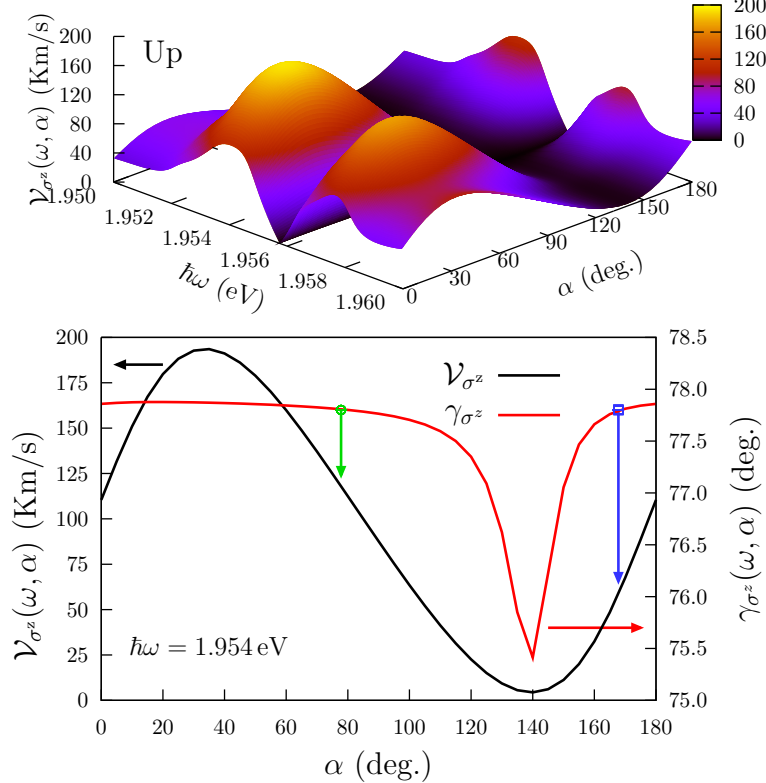


FIG. 5: For the Up structure, the top panel shows $\mathcal{V}_{\sigma^z}(\omega, \alpha)$ vs. $\hbar\omega$ and α , and the bottom panel shows $\gamma_{\sigma^z}(\omega, \alpha)$ (right scale, red line), and $\mathcal{V}_{\sigma^z}(\omega, \alpha)$ (left scale, black line), vs. α , for $\hbar\omega = 1.954$ eV, i.e. along the highest ridge shown in the 3D plot.

2. Alt structure

We proceed to analyze the Alt structure, just as we did with the Up structure, but in this case, we only choose the lower energy range shown in the left central panel of Fig. 3. In the top panel of Fig. 6, we plot $\mathcal{V}_{\sigma^z}(\omega, \alpha)$ vs. $0.715 \text{ eV} \leq \hbar\omega \leq 0.725 \text{ eV}$ and $0^\circ \leq \alpha \leq 180^\circ$. We see a broad peak that maximizes at $\alpha = 150^\circ$ and $\hbar\omega = 0.720$ eV, with a value of $\mathcal{V}_{\sigma^z}(\omega, \alpha) = 644.9$ Km/s. In the bottom panel, we show $\mathcal{V}_{\sigma^z}(\omega, \alpha)$ vs. α (left scale, black line), at $\hbar\omega = 0.720$ eV, thus following the highest ridge shown in the 3D plot of the top panel. Also, we plot the corresponding velocity angle $\gamma_{\sigma^z}(\omega, \alpha)$ (right scale, red line), where now we see that $\gamma_{\sigma^z}(\omega, \alpha)$ is centered at 109.2° having variations of $\pm 1.0^\circ$ for $0^\circ \leq \alpha \leq 180^\circ$. In this case, we find that $\gamma_{\sigma^z}^{\parallel}(\omega, \alpha) = \alpha = 108.8^\circ$, with $\mathcal{V}_{\sigma^z}(\omega, \alpha) = 450.05$ Km/s (see green arrow), and that from Eq. (17), $\gamma_{\sigma^z}^{\perp}(\omega, \alpha) = \alpha - 90^\circ = 110.0^\circ$, gives $\alpha = 20.0^\circ$, with $\mathcal{V}_{\sigma^z}(\omega, \alpha) = 60.84$ Km/s (see blue arrow). Thus, as for the Up structure, we could inject electrons with a fixed spin which move parallel or perpendicular to the incident electric field.

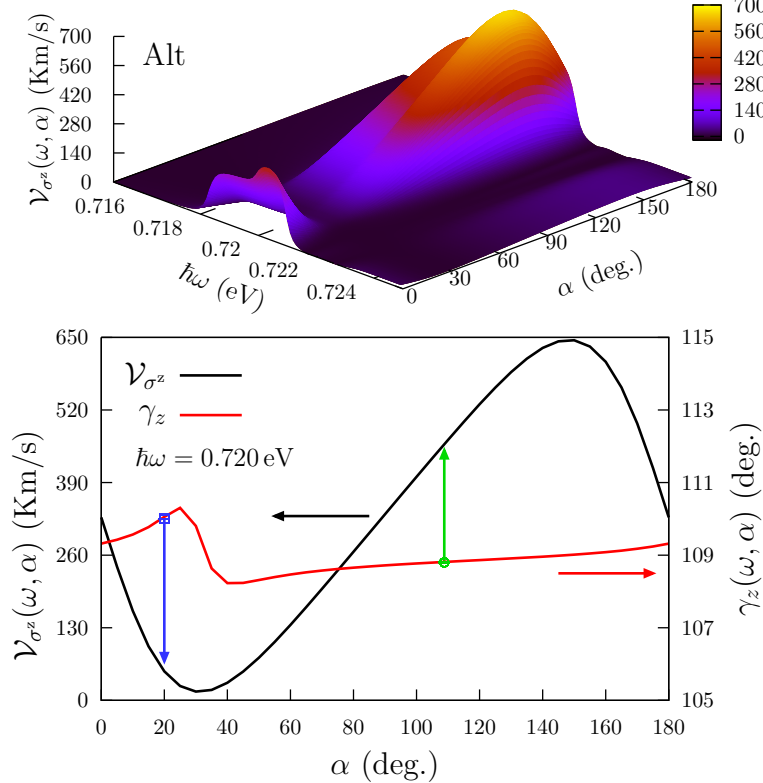


FIG. 6: For the Alt structure, the top panel shows $\mathcal{V}_{\sigma^z}(\omega, \alpha)$ vs. $\hbar\omega$ and α , and the bottom panel shows $\gamma_{\sigma^z}(\omega, \alpha)$ (right scale, red line), and $\mathcal{V}_{\sigma^z}(\omega, \alpha)$ (left scale, black line), vs. α , for $\hbar\omega = 0.720$ eV, i.e. along the ridge shown in the 3D plot.

C. Fixing velocity

We calculated $\mathcal{V}_a(\omega, \alpha)$ (Eq. (18)) fixing the electron velocity direction, a , to the x or y direction along the surface of the Up and Alt structures. From Eqns. (19) and (20), we determined the polar, $\theta_a(\omega, \alpha)$, and azimuthal, $\varphi_a(\omega, \alpha)$, angles corresponding to the direction of the spin.

1. Up structure

For the Up structure, we find once again that $\alpha = 35^\circ$ maximizes the response. In Fig. 7, we plot $\mathcal{V}_a(\omega, \alpha)$ (left scale, black line), $\theta_a(\omega, \alpha)$ (right scale, red line), and $\varphi_a(\omega, \alpha)$, (right scale, blue line), vs. $\hbar\omega$, for $a = x, y$. We see that for $\hbar\omega = 0.084$ eV, the response has a maximum of $\mathcal{V}_x(\omega, \alpha) = 431.7$ Km/s, with $\theta_x(\omega, \alpha) = 42.5^\circ$, and $\varphi_x(\omega, \alpha) = 208.3^\circ$, and $\mathcal{V}_y(\omega, \alpha) = 687.9$ Km/s, with $\theta_y(\omega, \alpha) = 13.9^\circ$, and $\varphi_y(\omega, \alpha) = 82.1^\circ$. This means that the spin is directed upward the third Cartesian quadrant of the xy plane when the electron moves along x , and is directed almost parallel

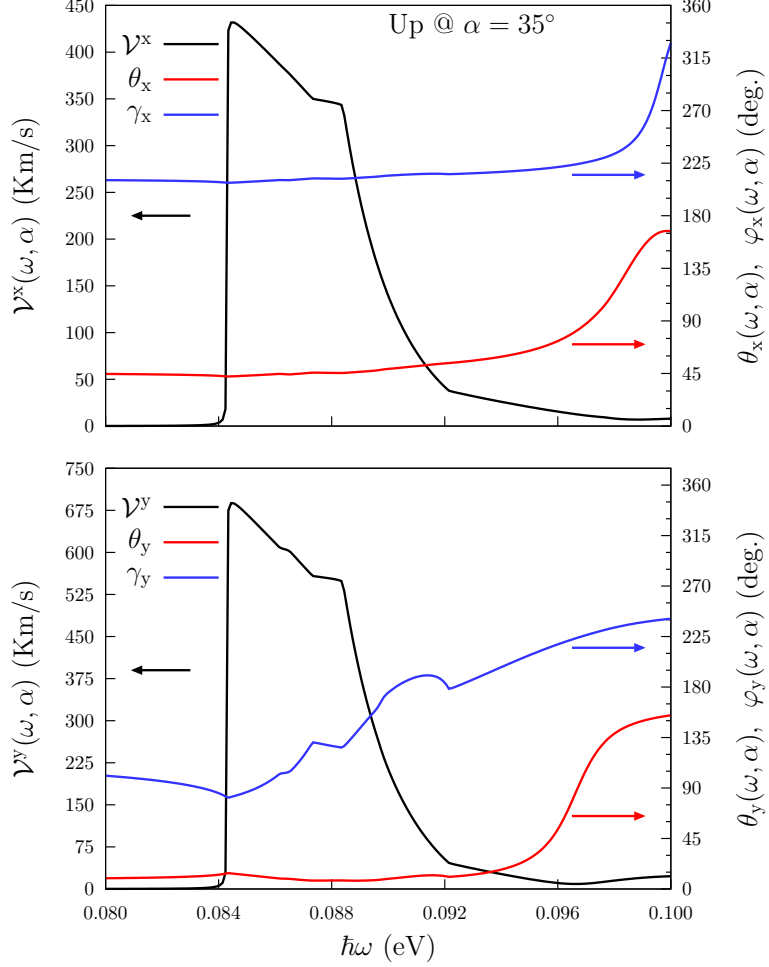


FIG. 7: For the Up structure, we show $\mathcal{V}_a(\omega, \alpha)$ (left scale, black line), $\theta_a(\omega, \alpha)$ (right scale, red line), and $\varphi_a(\omega, \alpha)$, (right scale, blue line), vs. $\hbar\omega$, for $\alpha = 35^\circ$, and $a = x, y$.

to the xy plane in the first quadrant when it moves along y . Also, from this figure we have that when the electron moves along x , the spin direction is almost constant for all the energies across the peak of the response, having $42.5^\circ < \theta_x(\omega, \alpha) < 53.7^\circ$ and $208.3^\circ < \varphi_x(\omega, \alpha) < 215.7^\circ$, and when the electron moves along y , the spin polar angle has again small variations, $11.3^\circ < \theta_y(\omega, \alpha) < 13.9^\circ$, but the azimuthal angle has significant variations, $82.1^\circ < \varphi_y(\omega, \alpha) < 182.4^\circ$.

In Fig. 8, we plot $\mathcal{V}_a(\omega, \alpha)$ vs. $\hbar\omega$, in the range where there are two local maxima at $\hbar\omega = 1.954$ eV and $\hbar\omega = 1.957$ eV. The former is the largest of the two, with $\mathcal{V}_x(\omega, \alpha) = 61.2$ Km/s, $\theta_x(\omega, \alpha) = 48.3^\circ$, and $\varphi_x(\omega, \alpha) = 54.3^\circ$, for the electron moving along x , and $\mathcal{V}_y(\omega, \alpha) = 293.2$ Km/s, $\theta_y(\omega, \alpha) = 49.8^\circ$, and $\varphi_y(\omega, \alpha) = 51.9^\circ$ for the electron moving along y . For the $\hbar\omega = 1.957$ eV peak, we obtain $\theta_x(\omega, \alpha) = 129.8^\circ$ and $\varphi_x(\omega, \alpha) = 231.7^\circ$, with $\mathcal{V}^x(\omega, \alpha) = 54.6$ Km/s and $\theta_y(\omega, \alpha) = 129.3$, and $\varphi_y(\omega, \alpha) = 230.7$, with $\mathcal{V}^y(\omega, \alpha) = 263.7$ Km/s.

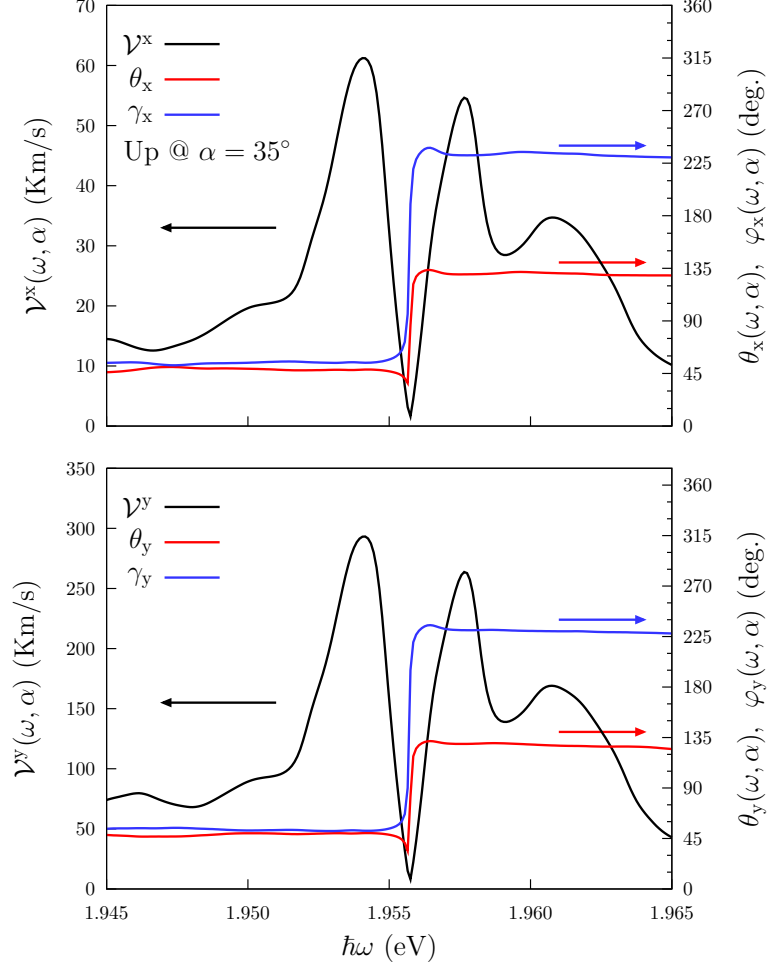


FIG. 8: For the Up structure we show $\mathcal{V}_a(\omega, \alpha)$ (left scale, black line), $\theta_a(\omega, \alpha)$ (right scale, red line), and $\varphi_a(\omega, \alpha)$, (right scale, blue line), vs. $\hbar\omega$, for $\alpha = 35^\circ$, and $a = x, y$.

We remark that these angles are almost constant for all the energy values across the peak of these two local maxima, for which the spin is directed upward in the first Cartesian quadrant of the xy plane when it moves along either x or y directions.

2. Alt structure

In Figs. 9 and 10, we plot $\mathcal{V}_a(\omega, \alpha)$ (left scale, black line), $\theta_a(\omega, \alpha)$ (right scale, red line), and $\varphi_a(\omega, \alpha)$, (right scale, blue line), vs. $\hbar\omega$ in two different ranges, and for $a = x, y$. In this case, $\alpha = 150^\circ$ maximizes both $\mathcal{V}_x(\omega, \alpha)$ and $\mathcal{V}_y(\omega, \alpha)$, as a function of α . In Fig. 9, the absolute maximum is at $\hbar\omega = 0.720$ eV, with $\mathcal{V}_x(\omega, \alpha) = 301.7$ Km/s, $\theta_x(\omega, \alpha) = 44.5^\circ$ and $\varphi_x(\omega, \alpha) = 51.2^\circ$, and $\mathcal{V}_y(\omega, \alpha) = 905.6$ Km/s, with $\theta_y(\omega, \alpha) = 119.7^\circ$ and $\varphi_y(\omega, \alpha) = 163.4^\circ$. Thus, the spin is directed upward the fourth Cartesian quadrant of the xy plane when the spin velocity is directed

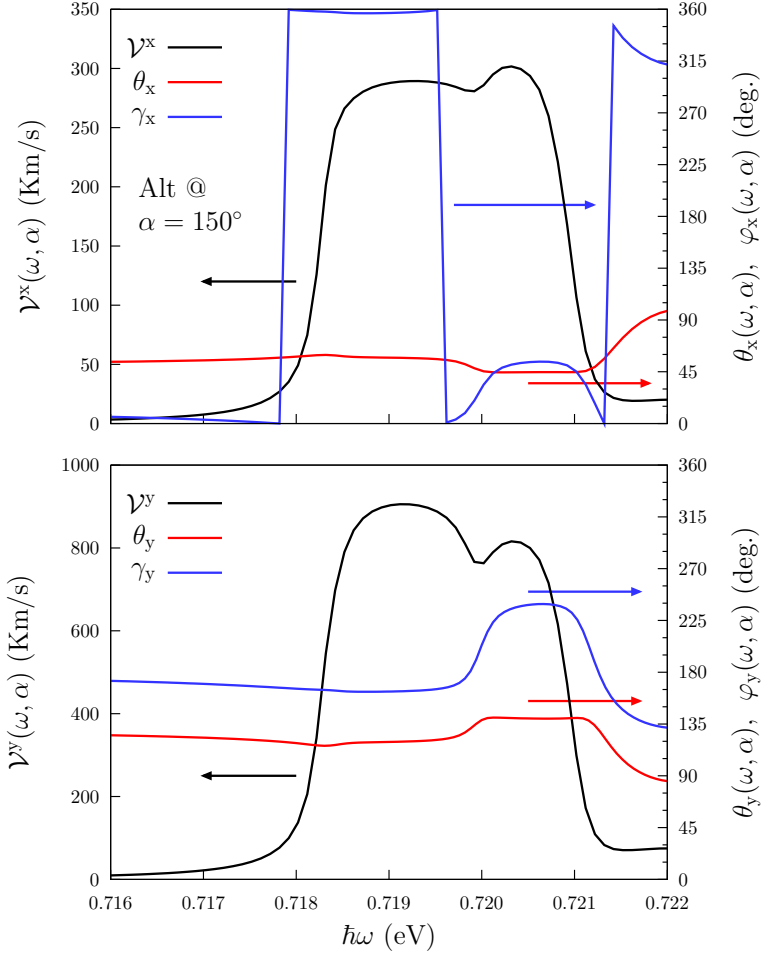


FIG. 9: For the Alt structure, we show $\mathcal{V}_a(\omega, \alpha)$ (left scale, black line), $\theta_a(\omega, \alpha)$ (right scale, red line), and $\varphi_a(\omega, \alpha)$, (right scale, blue line), vs. $\hbar\omega$, for $\alpha = 150^\circ$, and $a = x, y$.

along x , and directed downward the second Cartesian quadrant when the spin velocity is directed along y . Finally, in Fig. 9, the absolute maximum is at $\hbar\omega = 0.911$ eV, with $\mathcal{V}_x(\omega, \alpha) = 276.3$ Km/s, $\theta_x(\omega, \alpha) = 154.6^\circ$, and $\varphi_x(\omega, \alpha) = 292.3^\circ$, and $\mathcal{V}_y(\omega, \alpha) = 468.6$ Km/s, with $\theta_y(\omega, \alpha) = 129.2^\circ$, and $\varphi_y(\omega, \alpha) = 228.3^\circ$, implying that the spin is directed downward the fourth Cartesian quadrant of the xy plane when the spin velocity is directed along x , and directed downward the third Cartesian quadrant when the spin velocity is directed along y .

IV. CONCLUSIONS

We performed an *ab initio* calculation for the SVI by one-photon absorption of linearly polarized light in the Up and Alt 2D hydrogenated graphene structures, and we made the calculation for the case when the spin is polarized in the z direction or when the velocity is directed along x or y ; this

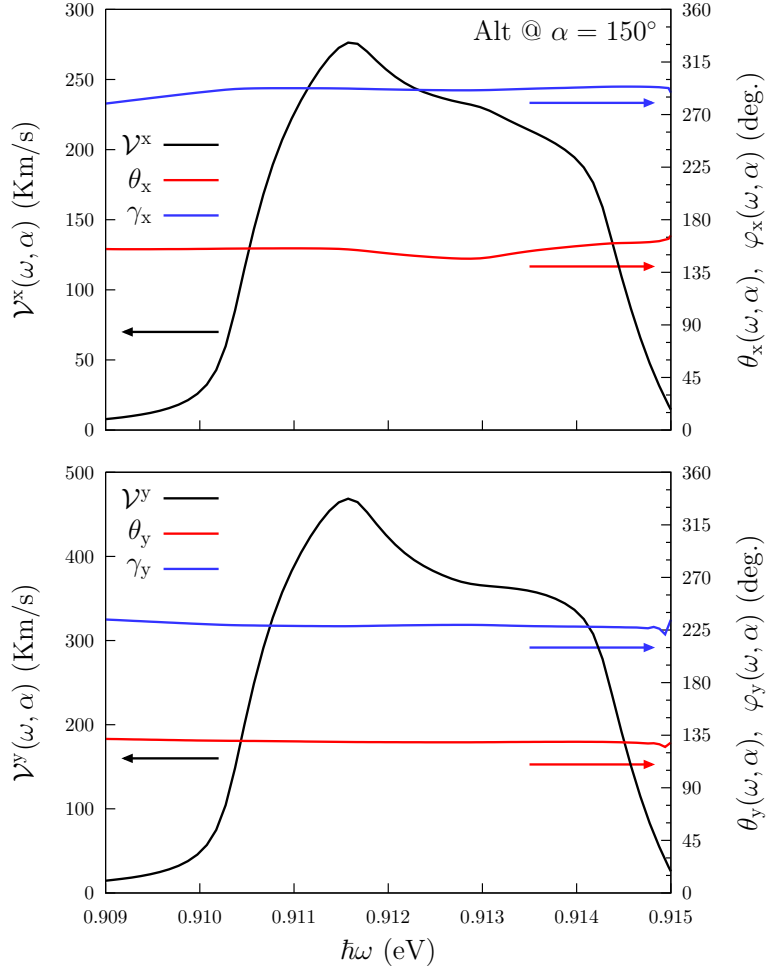


FIG. 10: For the Alt structure, we show $\mathcal{V}_a(\omega, \alpha)$ (left scale, black line), $\theta_a(\omega, \alpha)$ (right scale, red line), and $\varphi_a(\omega, \alpha)$, (right scale, blue line), vs. $\hbar\omega$, for $\alpha = 150^\circ$, and $a = x, y$.

effect does not seem to have been previously reported in this kind of structures. This SVI is very sensitive to the symmetry characteristics of the structures, presenting an anisotropic behavior. We found that the Up structure has the most intense response for the spin directed along z , resulting in $\mathcal{V}_{\sigma^z}(\omega, \alpha) = 668.0$ Km/s, and for an energy of the incoming beam of 0.084 eV. Also, the Alt structure has the most intense response when the spin moves along the y direction, resulting in $\mathcal{V}^y(\omega, \alpha) = 905.6$ Km/s for an energy of the incoming beam of 0.720 eV. The speed values obtained here are of the same order of magnitude as those of Ref. 13 in unbiased semiconductor quantum well structures. The spin relaxation time in pure and doped graphene is long enough in the order from nanoseconds to milliseconds.^{40,41} Then, according to our results, both are excellent candidates for the development of spintronics devices that require PSC due to the high spin velocity transport.

V. ACKNOWLEDGMENT

This work has been supported by *Consejo Nacional de Ciencia y Tecnología* (CONACyT), México, Grant No. 153930. R.Z.P. thanks CONACyT for scholarship support.

- ¹ S. A. Wolf, D. D. Awschalom, R. A. Buhrman, J. M. Daughton, S. Von Molnar, M. L. Roukes, A. Y. Chtchelkanova, and D. M. Treger, *Science* **294**, 1488 (2001).
- ² J. Fabian, A. Matos-Abiague, C. Ertler, P. Stano, and I. Zutic, *Ac. Phys. Slov.* (2007).
- ³ D. D. Awschalom and M. E. Flatté, *Nat. Phys.* **3**, 153 (2007).
- ⁴ S. Majumdar, R. Laiho, P. Laukkanen, I. J. Väyrynen, H. S. Majumdar, and R. Österbacka, *App. Phys. Lett.* **89**, 122114 (2006).
- ⁵ S. Datta and B. Das, *App. Phys. Lett.* **56**, 665 (1990).
- ⁶ M. Götte, M. Joppe, and T. Dahm, *Scientific Reports* **6** (2016).
- ⁷ Y. V. Pershin and M. Di Ventra, *Phys. Rev. B* **78**, 113309 (2008).
- ⁸ D. D. Awschalom, D. Loss, and N. Samarth, *Semiconductor Spintronics and Quantum Computation* (Springer Science & Business Media, 2013).
- ⁹ S. Murakami, N. Nagaosa, and S. C. Zhang, *Science* **301**, 1348 (2003).
- ¹⁰ A. Malshukov, C. Tang, C. Chu, and K.-A. Chao, *Phys. Rev. B* **68**, 233307 (2003).
- ¹¹ J. Sinova, D. Culcer, Q. Niu, N. A. Sinitsyn, T. Jungwirth, and A. H. MacDonald, *Phys. Rev. Lett.* **92**, 126603 (2004).
- ¹² R. D. R. Bhat and J. E. Sipe, *Phys. Rev. Lett.* **85**, 5432 (2000).
- ¹³ A. Najmaie, R. D. R. Bhat, and J. E. Sipe, *Phys. Rev. B* **68**, 165348 (2003).
- ¹⁴ R. D. R. Bhat, F. Nastos, A. Najmaie, and J. E. Sipe, *Phys. Rev. Lett.* **94**, 096603 (2005).
- ¹⁵ H. Zhao, E. J. Loren, H. M. Van Driel, and A. L. Smirl, *Phys. Rev. lett.* **96**, 246601 (2006).
- ¹⁶ M. J. Stevens, A. L. Smirl, R. D. R. Bhat, A. Najmaie, J. E. Sipe, and H. M. Van Driel, *Phys. Rev. Lett.* **90**, 136603 (2003).
- ¹⁷ T. Kimura, N. Hashimoto, S. Yamada, M. Miyao, and K. Hamaya, *NPG Asia Mat.* **4**, e9 (2012).
- ¹⁸ H. B. Heersche, P. Jarillo-Herrero, J. B. Oostinga, L. M. K. Vandersypen, and A. F. Morpurgo, *Nature* **446**, 56 (2007).
- ¹⁹ A. Geim and K. Novoselov, *Nat. Mater.* **6**, 183 (2007).
- ²⁰ A. Reina, X. Jia, J. Ho, D. Nezich, H. Son, V. Bulovic, M. Dresselhaus, and J. Kong, *Nano Lett.* **9**, 30 (2008).
- ²¹ K. S. Novoselov, Z. Jiang, Y. Zhang, S. V. Morozov, H. L. Stormer, U. Zeitler, J. C. Maan, G. S. Boebinger, P. Kim, and A. K. Geim, *Science* **315**, 1379 (2007).
- ²² A. Balandin, S. Ghosh, W. Bao, I. Calizo, D. Teweldebrhan, F. Miao, and C. Lau, *Nano Lett.* **8**, 902

(2008).

- ²³ Y. Zhang, T. Tang, C. Girit, Z. Hao, M. Martin, A. Zettl, M. Crommie, Y. Shen, and F. Wang, *Nature* **459**, 820 (2009).
- ²⁴ M. Han, B. Özyilmaz, Y. Zhang, and P. Kim, *Phys. Rev. Lett.* **98**, 206805 (2007).
- ²⁵ Z. Ni, T. Yu, Y. Lu, Y. Wang, Y. P. Feng, and Z. Shen, *ACS Nano* **2**, 2301 (2008).
- ²⁶ D. Wei, Y. Liu, Y. Wang, H. Zhang, L. Huang, and G. Yu, *Nano lett.* **9**, 1752 (2009).
- ²⁷ B. Guo, L. Fang, B. Zhang, and J. R. Gong, *Ins. J.* **1**, 80 (2011).
- ²⁸ C. Coletti, C. Riedl, D. S. Lee, B. Krauss, L. Patthey, K. von Klitzing, J. H. Smet, and U. Starke, *Phys. Rev. B* **81**, 235401 (2010).
- ²⁹ A. Varykhalov, M. R. Scholz, T. K. Kim, and O. Rader, *Phys. Rev. B* **82**, 121101 (2010).
- ³⁰ D. C. Elias, R. R. Nair, T. M. G. Mohiuddin, S. V. Morozov, P. Blake, M. P. Halsall, A. C. Ferrari, D. W. Boukhvalov, M. I. Katsnelson, A. K. Geim, et al., *Science* **323**, 610 (2009).
- ³¹ N. P. Guisinger, G. M. Rutter, J. N. Crain, P. N. First, and J. A. Stroscio, *Nano Lett.* **9**, 1462 (2009).
- ³² D. K. Samarakoon and X. Q. Wang, *ACS Nano* **4**, 4126 (2010).
- ³³ R. Zapata-Peña, S. M. Anderson, B. S. Mendoza, and A. I. Shkrebtii, *physica status solidi (b)* **253**, 226 (2016).
- ³⁴ S. F. Alvarado, H. Riechert, and N. E. Christensen, *Phys. Rev. Lett.* **55**, 2716 (1985).
- ³⁵ B. Schmiedeskamp, B. Vogt, and U. Heinzmann, *Phys. Rev. Lett.* **60**, 651 (1988).
- ³⁶ F. Nastos, B. Olejnik, K. Schwarz, and J. E. Sipe, *Phys. Rev. B* **72**, 045223 (2005).
- ³⁷ F. Nastos, J. Rioux, M. Strimas-Mackey, B. S. Mendoza, and J. E. Sipe, *Phys. Rev. B* **76**, 205113 (2007).
- ³⁸ X. Gonze, B. Amadon, P. M. Anglade, J. M. Beuken, F. Bottin, P. Boulanger, F. Bruneval, D. Caliste, R. Caracas, M. Côté, et al., *Comput. Phys. Commun.* **180**, 2582 (2009).
- ³⁹ C. Hartwigsen, S. Goedecker, and J. Hutter, *Phys. Rev. B* **58**, 3641 (1998).
- ⁴⁰ M. Wojtaszek, I. J. Vera-Marun, T. Maassen, and B. J. van Wees, *Phys. Rev. B* **87**, 081402 (2013).
- ⁴¹ C. Ertler, S. Konschuh, M. Gmitra, and J. Fabian, *Phys. Rev. B* **80**, 041405 (2009).